



HAL
open science

Effect of distance-dependent dispersivity on density-driven flow in porous media

Anis Younes, Marwan Fahs, Behzad Ataie-Ashtiani, Craig T. Simmons

► **To cite this version:**

Anis Younes, Marwan Fahs, Behzad Ataie-Ashtiani, Craig T. Simmons. Effect of distance-dependent dispersivity on density-driven flow in porous media. *Journal of Hydrology*, 2020, 589, pp.125204. <10.1016/j.jhydrol.2020.125204>. <hal-03044976>

HAL Id: hal-03044976

<https://hal.science/hal-03044976v1>

Submitted on 9 Dec 2020

HAL is a multi-disciplinary open access archive for the deposit and dissemination of scientific research documents, whether they are published or not. The documents may come from teaching and research institutions in France or abroad, or from public or private research centers.

L'archive ouverte pluridisciplinaire **HAL**, est destinée au dépôt et à la diffusion de documents scientifiques de niveau recherche, publiés ou non, émanant des établissements d'enseignement et de recherche français ou étrangers, des laboratoires publics ou privés.



HAL Authorization

1
2
3
4
5
6
7
8
9
10
11
12
13
14
15
16
17
18
19
20
21
22

Effect of distance-dependent dispersivity on density-driven flow in porous media

Anis Younes^{1,2,3}, Marwan Fahs¹, Behzad Ataie-Ashtiani^{4,5}, Craig T. Simmons⁵

¹ LHyGES, Univ. de Strasbourg/EOST/ENGEES, CNRS, 1 rue Blessig, 67084 Strasbourg, France.

² LISAH, Univ Montpellier, INRA, IRD, Montpellier SupAgro, Montpellier, France.

³ LMHE, Ecole Nationale d'Ingénieurs de Tunis, Tunisie

⁴ Department of Civil Engineering, Sharif University of Technology, PO Box 11155-9313, Tehran, Iran

⁵ National Centre for Groundwater Research and Training, College of Science and Engineering, Flinders University, GPO Box 2100, Adelaide, SA 5001, Australia

Submitted to *Journal of Hydrology*

*Contact person: Marwan Fahs

E-mail : fahs@unistra.fr

23 ***Abstract***

24 In this study, the effect of distance-dependent dispersion coefficients on density-driven flow is
25 investigated. The linear asymptotic model, which assumes that dispersivities increase linearly
26 with distance from the source of contamination and reach asymptotic values at a large
27 asymptotic distance, is employed. An in-house numerical model is adapted to handle distance-
28 dependent dispersion. The effect of asymptotic-dispersion on aquifer contamination is analyzed
29 for two tests: (i) a seawater intrusion problem in a coastal aquifer and (ii) a leachate transport
30 problem from a surface deposit site. Global Sensitivity Analysis (GSA) combined with the
31 Polynomial Chaos Expansion (PCE) surrogate modelling is conducted to assess the influence
32 of the dispersion coefficients on the contamination plume for both configurations.

33 For the seawater intrusion problem, the results show that the length of the toe is mainly
34 controlled by the asymptotic transverse dispersivity whereas the spread of the concentration is
35 sensitive to the asymptotic longitudinal dispersivity and the asymptotic dispersivity distance.
36 The latter is the most important parameter controlling the amount of salt which intrudes into
37 the aquifer. For the leachate transport problem, the results show that the asymptotic longitudinal
38 dispersivity coefficient does not affect the concentration distribution. The asymptotic
39 dispersivity distance has a strong effect on the total amount of contaminant that enters the
40 aquifer. This effect can be three times more important than the effect of the asymptotic
41 transverse dispersivity. These findings are likely to be helpful for the investigation and
42 management of density-driven flow problems.

43 **Keywords**

44 Density driven flow, saltwater intrusion, leachate transport, variable dispersion, asymptotic
45 model, global sensitivity analysis.

46

47

48 **1. Introduction**

49 Density-driven flow (DDF) is a particular configuration of transport in porous media in which
50 the fluid concentration causes a change in groundwater density which can significantly affect
51 the flow dynamics. DDF can be encountered in several applications related to contaminant
52 transport in aquifers. Among these applications, a well-known problem is the contamination of
53 coastal aquifers by saltwater intrusion (Werner et al., 2013) which is a major concern around
54 the world. Another important example is groundwater contamination by leachates from surface
55 industrial waste and landfills (Frind, 1982). Managing and predicting the evolution of pollutants
56 in such situations require accurate numerical simulations.

57 The simulation of DDF problems is based on coupling Darcy's groundwater flow equation to
58 the solute transport equation via a state relation expressing the density as a function of solute
59 concentration. Transport of solute in the aquifer is ruled by advection, representing the solute
60 displacement by the mean fluid flow, and by dispersion, which accounts for solute spreading
61 caused by velocity variations due to the heterogeneity of the porous medium at different scales
62 (Liu et Kitandis, 2013; Kitanidis, 2017; Dai et al., 2020). Dispersion processes have been found
63 to play a major role in DDF problems as they cause mixing between different fluids. The effect
64 of dispersion on DDF has been widely investigated in the literature. For instance, Abarca et al.
65 (2007) studied the effect of dispersion on DDF in the context of seawater intrusion and showed
66 that when dispersion is taken into account, concentration isolines resemble those observed in
67 real coastal aquifers. Emami-Meybodi (2017) studied instabilities driven by dispersion for an
68 unstable DDF problem with mixed convective flow. Wen et al. (2018) defined a dispersive
69 Rayleigh number and investigated the effect of dispersion on the Rayleigh-Darcy convection
70 problem. Fahs et al. (2020) investigated the effect of dispersion on thermal DDF problem.

71 In most DDF models, dispersion is ruled using a velocity-dependent dispersion tensor involving
72 constant coefficients characterizing mixing in the longitudinal (parallel to the flow) and

73 transverse (orthogonal to flow) directions. In the last decades, many studies have shown that
74 this conventional approach cannot satisfactorily represent field transport especially for aquifers
75 with spatial heterogeneity (Pickens and Grisak, 1981a). Alternative approaches have developed
76 such as stochastic models (e.g. Gelhar, 1992; Zhang, 2002, Kerrou and Renard, 2010; Pool et
77 al., 2015) or continuous time random walk methods (e.g. Berkowitz et al., 2000; Dentz et al.,
78 2004). However, these methods usually require sufficient field measurements to formulate
79 statistical structure and are known to be computationally expensive (Wang et al., 2006). Such
80 difficulties have motivated using the conventional dispersion approach, but by considering that
81 the dispersivity values are temporal or scale dependent (Pickens and Grisak, 1981a). In other
82 words, the longitudinal and transverse dispersion coefficients are not constant but can vary with
83 the distance from the source of contamination. Indeed, in a tracer test, Molz et al. (1983) found
84 that dispersivity is not constant but increases with the travel distance because of the scale
85 dependence of dispersivities. This phenomenon has been observed both in field-scale transport
86 (e.g. Pickens and Grisak 1981a; Gelhar et al., 1992; Schulze-Makuch, 2005) and laboratory-
87 scale transport (e.g., Silliman and Simpson, 1987; Khan and Jury, 1990; Huang et al., 1995;
88 Vanderborght and Vereecken, 2007). According to Gao et al. (2012), the scale dependence of
89 dispersivity can be related to different processes such as the heterogeneity of the porous media
90 at different scales (Gelhar et al., 1992; Huang et al., 2006), the fractal nature of the pore space
91 in the aquifer (Wheatcraft and Tyler, 1988) or the anomalous transport (Cortis and Berkowitz,
92 2004). Mishra and Parker (1990) showed that a hyperbolic dispersivity-distance function allows
93 a good fitting of the data estimated from a natural gradient tracer experiment. Kangle et al.
94 (1996) provided a one-dimensional analytical solution with linear asymptotic dispersion. Chen
95 et al. (2003, 2007) investigated distance-dependent dispersion for convergent and divergent
96 flow fields with linear scale-dependent dispersion. Chen et al (2008a) studied one-dimensional
97 transport with hyperbolic asymptotic dispersivity function. Pérez Guerrero and Skaggs (2010)

98 derived a general analytical solution for one-dimensional transport with distance-dependent
99 coefficients. Gao et al. (2010, 2012) investigated mobile-immobile transport model with
100 asymptotic scale-dependent dispersivity. You and Zhan (2013) developed semi-analytical
101 solutions for solute transport in a finite column with linear asymptotic and exponential distance-
102 dependent dispersivities and time-dependent sources.

103 Thus, in the literature, the effect of asymptotic dispersivity has been essentially investigated for
104 simplified situations of 1D transport (e.g. Basha and El-Habel, 1993; Yates, 1992; David-
105 Logan, 1996; Pang and Hunt, 2001; Chen et al., 2003; Pérez Guerrero and Skaggs, 2010;
106 Sharma and Abgaze, 2015, Wang et al., 2019), 2D problems with a uniform flow field (e.g.
107 Hunt, 2002; Chen et al., 2008b) or radially convergent divergent flow fields (e.g. Chen et al.,
108 2003, 2006, 2007). To the best our knowledge, investigation of distance-dependent dispersion
109 coefficients in cases involving complex velocity fields, such as in DDF problems, have not been
110 undertaken.

111 The aim of this work is to incorporate distance-dependent dispersion in a DDF model and to
112 investigate the effect of dispersion parameters on contaminant transport. As conceptual models,
113 we consider (i) the Henry problem describing seawater intrusion (SWI) in a coastal aquifer
114 (Henry, 1964) and (ii) the leachate transport problem proposed by Frind (1982) to investigate
115 the leachate plume from a surface deposit site. The effect of distance-dependent dispersivities
116 on the aquifer contamination is investigated using Global Sensitivity Analysis (GSA) combined
117 with Polynomial Chaos Expansion (PCE) surrogate modelling (Sudret, 2008; Fajraoui et al.,
118 2012, 2017; Mara et al., 2017).

119 **2. Methods**

120 2.1 The mathematical model and numerical code

121 The mathematical model for water movement through porous media is based on the mass
122 conservation equation and Darcy's law (Guevara et al., 2015):

123
$$\rho S \frac{\partial h}{\partial t} + \varepsilon \frac{\partial \rho}{\partial C} \frac{\partial C}{\partial t} + \rho \nabla \cdot \mathbf{q} = 0 \quad (1)$$

124
$$\mathbf{q} = -\frac{\rho_0 g}{\mu} \mathbf{k} \left(\nabla h + \frac{\rho - \rho_0}{\rho_0} \nabla z \right) \quad (2)$$

125 where ρ is the fluid density [ML⁻³], S the specific mass storativity related to head changes [L⁻¹], h the equivalent freshwater head [L], t the time [T], ε the porosity [-], C the relative concentration [-], \mathbf{q} the Darcy's velocity [LT⁻¹], ρ_0 the density of the displaced fluid [ML⁻³], g the gravity acceleration [LT⁻²], μ the fluid dynamic viscosity [ML⁻¹T⁻¹], \mathbf{k} the permeability tensor [L²] and z the depth [L] taken positive upwards.

130 The contaminant transport in porous media is based on the solute mass conservation equation:

131
$$\frac{\partial(\varepsilon \rho C)}{\partial t} + \nabla \cdot (\rho C \mathbf{q} - \rho \mathbf{D} \cdot \nabla C) = 0 \quad (3)$$

132 where the dispersive tensor \mathbf{D} is given by:

133
$$\mathbf{D} = D_m \mathbf{I} + (\alpha_L - \alpha_T) \mathbf{q} \mathbf{q}^T / |\mathbf{q}| + \alpha_T |\mathbf{q}| \mathbf{I} \quad (4)$$

134 with α_L and α_T the longitudinal and transverse dispersion coefficients [L], D_m the pore water diffusion coefficient [L²T⁻¹] and \mathbf{I} the unit tensor. The associated boundary conditions of the flow-transport system (1)-(3) are of Dirichlet, Neuman or mixed type.

137 Flow and transport equations are coupled via the linear mixture density equation:

138
$$\rho = \rho_0 + (\rho_1 - \rho_0) C \quad (5)$$

139 where ρ_1 is density of contaminant.

140 In this work, we assume that the longitudinal and transverse dispersion coefficients are a function of the distance from the source of contamination. Distance-dependent dispersivities are generally ruled using one of the four types of functions suggested by Pickens and Grisak (1981b) including linear, parabolic, asymptotic and exponential functions. The linear distance-dependent dispersivity function has been largely used in the literature (e.g. Pang and Hunt,

145 2001; Gao et al., 2010; Pérez Guerrero and Skaggs, 2010; Chen et al., 2008b). However, this
 146 function seems to be unphysical, because field observations show that a constant dispersivity
 147 could be asymptotically reached (Gelhar et al., 1992; Picken and Grisak, 1981a). Huang et al.
 148 (1995) used a linear-asymptotic distance-dependent function where the dispersivity value
 149 increases linearly with the transport distance and reaches an asymptotic value at a certain large
 150 distance. The linear-asymptotic model was adopted by You and Zhan (2013) and is employed
 151 in this work:

$$152 \quad \alpha_{L,T}(\mathbf{x}) = \begin{cases} \alpha_{L,T}^0 \frac{\ell}{\ell_0}, & 0 \leq \ell \leq \ell_0 \\ \alpha_{L,T}^0, & \ell_0 \leq \ell \end{cases} \quad (6)$$

153 where ℓ corresponds to the distance from the source of contamination, α_L^0 and α_T^0 are
 154 respectively the asymptotic longitudinal and transverse dispersion coefficients and ℓ_0 is the
 155 asymptotic distance after which both longitudinal and transverse dispersivities reach their
 156 asymptotic values $\alpha_{L,T} = \alpha_{L,T}^0$.

157 The coupled flow-transport system is solved with an advanced in-house numerical model using
 158 triangular meshes (Ackerer and Younes, 2008). The flow equations (Eqs. 1-2) are solved by the
 159 mixed finite element method (Younes et al., 2010). The transport equation (Eq. 3) is solved by
 160 combining two numerical methods: Discontinuous Galerkin (DG) method for solving advection
 161 and Multipoint Flux Approximation (MPFA) method for solving dispersion. Coupling between
 162 flow and transport equations is performed using the non-iterative scheme proposed in Younes
 163 and Ackerer (2010) with proper time management. This scheme was shown to be highly
 164 efficient and more accurate than the standard iterative procedure. The in-house code has been
 165 validated by comparison against semi-analytical solutions in Fahs et al. (2016). Performance
 166 and robustness of the code has been highlighted in Shao et al. (2018) by comparison against
 167 COMSOL Multiphysics. In this work, the in-house code is modified to handle distance-

168 dependent dispersion coefficients. Both longitudinal and transverse dispersivities are defined
169 elementwise and their values are calculated using (Eq. 4) where ℓ corresponds to the distance
170 from the center of each element to the source of contamination.

171
172 2.2 The Henry saltwater Intrusion Problem

173 Real applications of SWI at a field scale are increasingly reported in the literature. However, in
174 several theoretical and applied studies, SWI is often investigated based on the hypothetical
175 Henry problem (Henry, 1964) (Figure 1a). This problem represents a common benchmark that
176 is widely used for multiple purposes as understanding physical processes, numerical model
177 verification, and parameter sensitivity analyses. A detailed review of the different use of the
178 Henry problem as a surrogate representation of SWI can be found in Werner et al. (2013) and
179 Fahs et al. (2018).

180 The Henry problem represents SWI in a vertical cross-section of a confined coastal aquifer
181 where an inland freshwater flow is in equilibrium with seawater that intrudes into the aquifer
182 from the seaside due to its higher density (Figure 1a). The first studies on the Henry problem
183 have been limited to pure molecular diffusion cases. More realistic configurations that include
184 velocity-dependent dispersion have been suggested in Abarca et al. (2007) and Fahs et al.
185 (2016). These cases will be considered here as this work deals with asymptotic dispersion
186 coefficients.

187

188

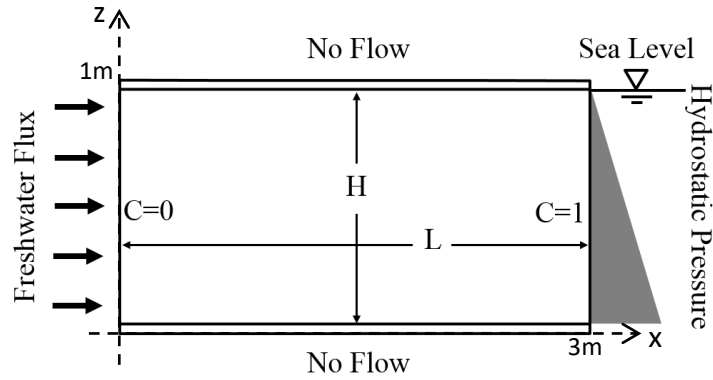
189

190

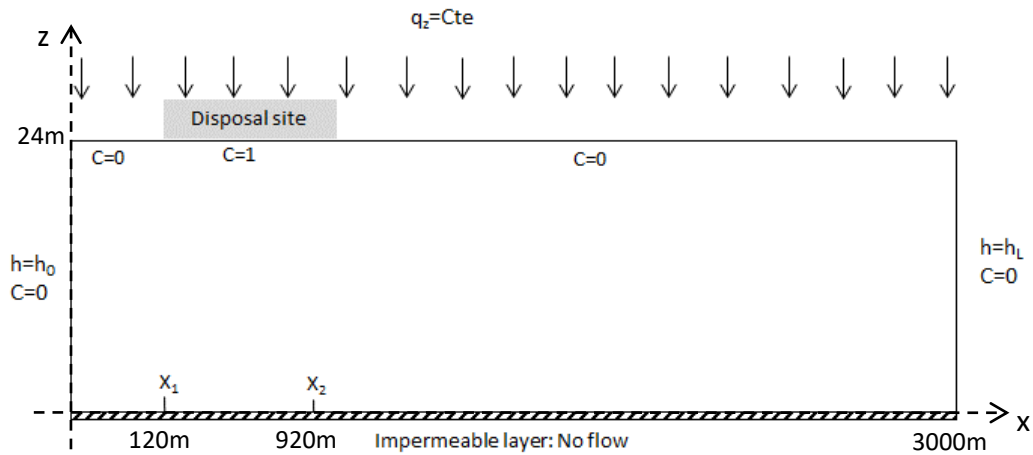
191

192

(a)



(b)



194 **Figure 1.** (a) Henry problem domain and boundary conditions; (b) The leachate transport
 195 problem (Frind, 1982).

196

197 Following Simpson and Clement (2004), we decrease the freshwater recharge by half to
 198 increase the density-dependent effects compared to boundary forces. Further, we use a larger

199 rectangular domain with an aspect ratio $\frac{L}{H} = 3$ as proposed by Zidane et al. (2012) to reduce

200 the influence of the left boundary condition on the saltwater distribution. The parameters and
 201 boundary conditions for the Henry problem are given in Table 1.

202

203

204

205

206
207
208
209
210

Table 1. Parameters and boundary conditions for the Henry problem.

permeability	$k = 1.0204 \times 10^{-9} \text{ m}^2$
porosity	$\varepsilon = 0.35$
length of the aquifer	$L = 3 \text{ m}$
height of the aquifer	$H = 1 \text{ m}$
-molecular diffusion coefficient	$D_m = 9.4 \times 10^{-8} \text{ m}^2 \text{ s}^{-1}$
Boundary conditions for flow	- hydrostatic pressure at the right hand side - constant flux at the inland boundary: $Q = 3.3 \times 10^{-5} \text{ m}^2/\text{s}$ - no flow along the top and bottom
Boundary conditions for transport	- $\rho_0 = 1000 \text{ kg/m}^3$ on the left boundary. - $\rho_1 = 1025 \text{ kg/m}^3$ on the right boundary - zero concentration gradient along the top and bottom

211
212
213
214
215
216
217

The numerical model is employed to analyze the saltwater intrusion by considering that uncertainty of model outputs is associated with the following dispersion parameters: the asymptotic longitudinal dispersivity α_L^0 , the asymptotic transverse dispersivity α_T^0 and the asymptotic distance ℓ_0 . Note that the longitudinal and transverse dispersivities are assumed to be independent. The corresponding uncertainty ranges (Table 2) are sufficiently large to explore the role of each parameter.

Table 2. Uncertainty ranges of the dispersion coefficients for the Henry problem.

Parameter	Uncertainty Range
α_L^0 [m]	[0.1, 1.0]
α_T^0 [m]	[0.04, 1.0]
ℓ_0 [m]	[0, 2.0]

219

220 2.3 The leachate transport problem in unconfined aquifer

221 This problem was proposed by Frind (1982) to investigate groundwater contamination by
 222 leachates from sanitary landfills or industrial waste disposal sites. A typical problem is
 223 considered (Figure 1b) where a disposal site unprotected from precipitation is situated above
 224 the water table in a rectangular unconfined aquifer of 3000 m length and 24m thickness.
 225 The parameters and boundary conditions are described in Table 3.

226 **Table 3.** Parameters and boundary conditions for the leachate transport problem.

- permeability	$k_x = 0.3262 \times 10^{-10} \text{ m}^2$ $k_z = 0.3262 \times 10^{-11} \text{ m}^2$
- porosity	$\varepsilon = 0.2$
- length of the aquifer	$L = 3000 \text{ m}$
- height of the aquifer	$H = 24 \text{ m}$
- molecular diffusion coefficient	$D_m = 0.0 \text{ m}^2 \text{ s}^{-1}$
- boundary conditions for flow	- fixed head at the left ($h_0=0$) and right ($h_L=-17.5\text{m}$) hand sides - constant flux at the top: $q_z = 30 \text{ cm/year}$ - no flow along the bottom
- boundary conditions for transport	- fixed relative concentration ($C=C_0$) at the top with $C_0=1$ for $x_1 \leq x \leq x_2$ $C_0=0$ elsewhere with $x_1 = 120 \text{ m}$ and $x_2 = 920 \text{ m}$ - fixed relative concentration ($C=0$) at the left and right hand sides - density of the contaminant $\rho_1 = 1007.1 \text{ kg/m}^3$ - zero concentration gradient along the bottom

227

228 Large uncertainty ranges (Table 4) are associated to the dispersion parameters (α_L^0 , α_T^0 and ℓ_0
 229) in order to investigate the role of each of them. Note that because the leachate transport
 230 problem has larger dimensions than the synthetic Henry problem, the dispersion parameters are
 231 allowed to have larger values than previously.

232

233

234

235 **Table 4.** Uncertainty ranges of the dispersion parameters for the leachate transport problem.

Parameter	Uncertainty Range
α_L^0 [m]	[0.1, 20.0]
α_T^0 [m]	[0.04, 5.0]
ℓ_0 [m]	[0, 50.0]

236

237 **3. Global sensitivity analysis**

238 Effect of the dispersion parameters on DDF is investigated using global sensitivity analysis
 239 (GSA). To this aim, the variance-based sensitivity indices of Sobol' (Sobol', 2001) are
 240 computed using Polynomial Chaos Expansion (PCE). The Sobol' indices measure the
 241 contribution of an input (alone or by interactions with other inputs) to the output variance. They
 242 are well adapted for GSA since they do not require any assumption of monotony or linearity of
 243 the model (Saltelli et al., 2006). Two Sobol' indices are noteworthy:

244 - the first-order sensitivity index,

$$245 \quad S_i = \frac{V[E[y|\chi_i]]}{V[y]} = \frac{V_i}{V} \quad (4)$$

246 - the total sensitivity index,

$$247 \quad ST_i = \frac{E[V[y|\chi_{-i}]]}{V[y]} = \frac{V_i^T}{V} \quad (5)$$

248 where y is the model output, χ is the set of parameters $\chi = (\alpha_L^0, \alpha_T^0, \ell_0)$, $E[]$ is the
 249 mathematical expectation (the average), $V[]$ is the mathematical variance, $E[|]$ and $V[|]$
 250 are their respective conditional forms. χ_i represents one of the parameters, and χ_{-i} stands for
 251 the set of parameters χ without the parameter χ_i .

252 The first-order sensitivity index (or main effect index) $S_i \in [0,1]$ measures the amount by which
 253 the variance of y is reduced when the true value of χ_i is known. The total sensitivity index
 254 $ST_i \in [0,1]$ measures the remaining uncertainty in y after all parameters are known except χ_i .
 255 It evaluates the contribution of χ_i to the response variance, including its interactions with the
 256 other parameters (i.e., χ_{-i}). If interactions between parameters are negligible, we have $\sum_i S_i = 1$
 257 and $S_i = ST_i, \forall i$.

258 The marginal effect $\bar{y}(\chi_i)$ of the parameter χ_i on the model output y enables to investigate
 259 the range of variation of y with respect to χ_i ,

$$260 \quad \bar{y}(\chi_i) = E[y|\chi_i]. \quad (7)$$

261 In this work, we use the Polynomial Chaos Expansion (PCE) surrogate modeling to infer
 262 sensitivity indices (Fajraoui et al., 2012, 2017; Younes et al., 2016; Shao et al., 2017). PCE
 263 allows an efficient evaluation of the Sobol' indices, since they can be easily calculated using
 264 the PCE coefficients (Sudret, 2008).

265 Since we deal with only three uncertain parameters (α_L^0, α_T^0 and ℓ_0), we use a full surrogate

266 PCE of order 4. The number of polynomial coefficients in the expansion is therefore $\frac{7!}{4! \times 3!} = 35$

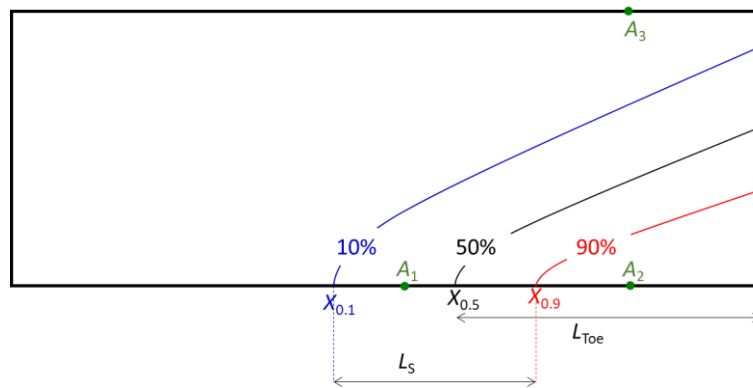
267 . The coefficients of the surrogate PCE are calculated by a least-square technique minimizing
 268 the sum of squared errors between model responses and the PCE. To this aim, a hundred of
 269 evaluations of the Henry and leachate transport problems are performed using parameter values
 270 randomly generated in the intervals of variation given in Table 2 and Table 4 respectively.

271 **4. Results for the Henry SWI problem**

272 A mesh converged solution is obtained a uniform triangular mesh formed by 4800 elements.
 273 The effect of the dispersion parameters on saltwater intrusion is investigated based on the
 274 following metrics (see Figure 2).

- 275 - The positions $X_{0.1}$, $X_{0.5}$ and $X_{0.9}$ of respectively the 10%, 50% and 90% isochlors at
 276 the aquifer bottom. Note that the $X_{0.5}$ is related to the well-known length of the toe L_{toe}
 277 which is the distance between the seaside boundary and $X_{0.5}$.
- 278 - The spread of the concentration $L_S = X_{0.9} - X_{0.1}$ which corresponds to the distance
 279 between the 10% and the 90% isochlors at the bottom of the domain.
- 280 - The total mass in the domain.
- 281 - The values of steady state concentration at the following selected points: $A_1(1.5,0)$;
 282 $A_2(2.5,0)$ and $A_3(2.5,1)$.

283



284

285 **Figure 2.** Seawater intrusion metrics used for the assessment of effects of the dispersion
 286 parameters.
 287

288 4.1 Salinity distribution

289 Figure 3a depicts the mean concentration values as well as the corresponding 10%, 50% and
 290 90% concentration contours. This figure shows that the distribution of the mean concentration
 291 reflects the general distribution of salinity in coastal aquifers which gives confidence to the
 292 accuracy of the PCE surrogate model. Saltwater intrudes from the right and reaches equilibrium

293 with the inland freshwater flow. Saltwater intrusion is more pronounced near the bottom
 294 because of density effects. The mean concentration distribution in Figure 3a shows a wide
 295 mixing zone due to the large uncertainty ranges of the dispersion parameters (Table 2).
 296



297 **Figure 3.** The Henry problem: (a) Spatial map of the mean concentration values (black lines
 298 represent 90%, 50% and 10% isochlors); (b) Spatial map of the variance of concentrations
 299 (dashed lines limit the zone of high variability- 5% of standard deviation).
 300

301 The distribution of the variance of the concentration shows that high variances regions are
 302 located at the center of the domain near the bottom of the aquifer (Figure 3b). This makes sense
 303 as the length of the toe is mainly controlled by the dispersion processes (Abarca et al., 2007;
 304 Fahs et al., 2016). Indeed, it is well known that low dispersion increases the buoyancy forces
 305 compared to dispersion effects and yields much more intrusion near the bottom of the aquifer
 306 (Younes and Fahs, 2014). This explains the high variance region near A1 in Figure 3b.
 307 Significant variability of the salinity can be observed also at top of the aquifer near the seaside
 308 (Figure 3b). In this zone, the groundwater flow is discharging to the sea. Thus, the salinity of

309 this zone is mainly due to dispersion. The dashed contour in Figure 3b shows the region where
310 the effect of dispersion parameters is significant which corresponds to 5% of the standard
311 deviation of the concentrations.

312

313 The spatial maps of first order Sobol' indices representing the sensitivity of the salinity
314 distribution to α_L^0 , α_T^0 and ℓ_0 are plotted in the Figure 4. For the region of significant variance
315 (the region delimited by the dashed lines), Figure 4a shows that α_L^0 has a negligible effect on
316 salinity distribution, except around A2 where a moderate effect can be observed. The parameter
317 α_T^0 is the most influential parameter as its zone of high sensitivity is situated in the region of
318 high variability (Figure 4b). Significant sensitivity to α_T^0 is observed around A3 but the highest
319 sensitivity area is situated in the mixing zone near A1. This is in agreement with the results of
320 Fahs et al. (2016) and is related to the fact that in this zone, the velocity field is not parallel to
321 the concentration gradient. As shown in Fahs et al. (2016), in such a case, the dispersion
322 processes are dominated by the transverse dispersion and hence, the salinity distribution is
323 highly sensitive to α_T^0 in this zone. The parameter ℓ_0 is influential near the seaside boundary
324 (Figure 4c) which makes sense since, far from the sea, the longitudinal and transverse dispersion
325 coefficients reach their asymptotic values and the salinity distribution become insensitive to ℓ_0

326 .

327

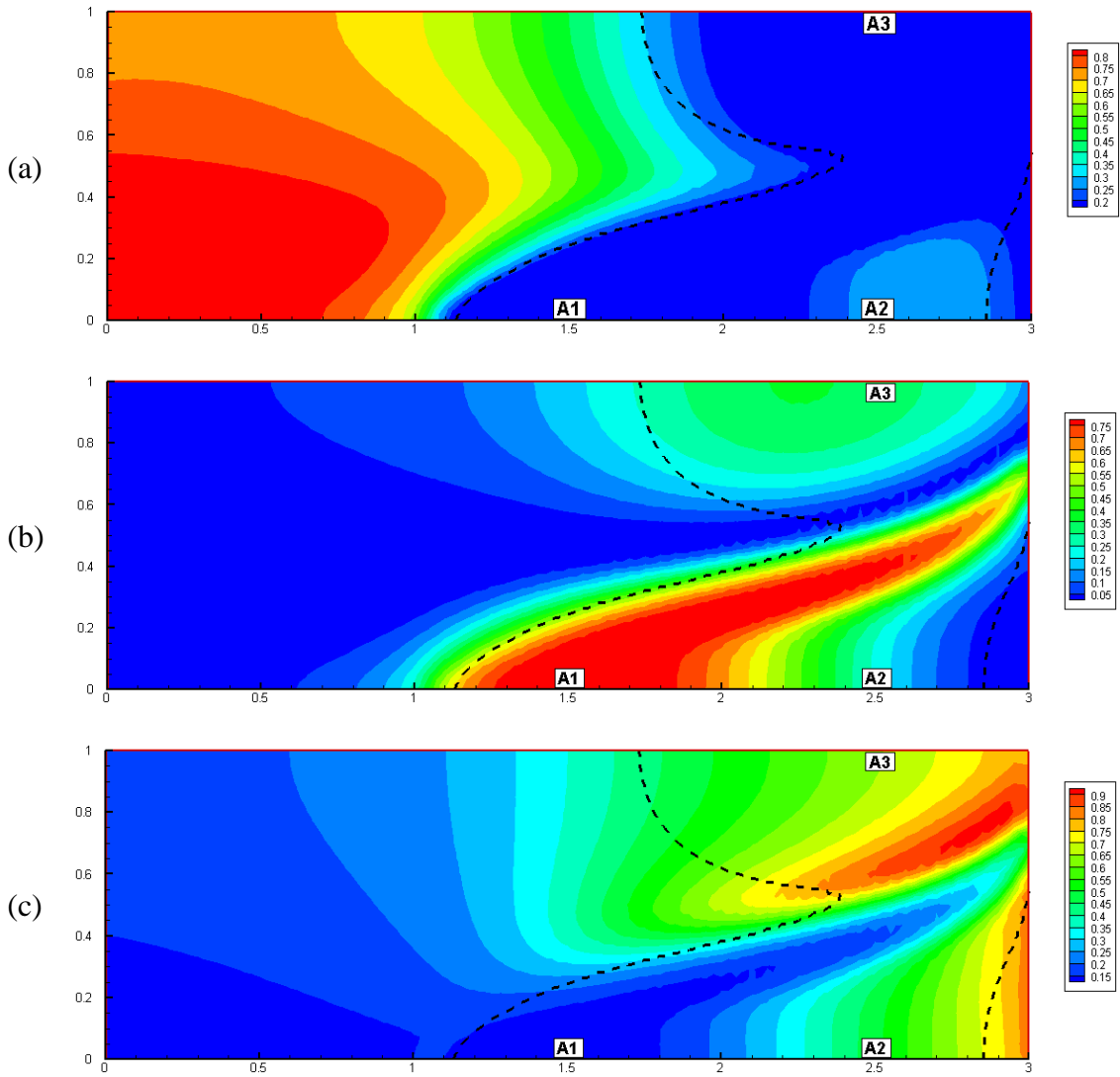
328

329

330

331

332



333 **Figure 4.** Spatial maps of the first-order sensitivity indices: (a) sensitivity of salinity
 334 distribution to α_L^0 , (b) sensitivity of salinity distribution to α_r^0 and (c) sensitivity of salinity
 335 distribution to ℓ_0 . Dashed lines limit the zone of high variability (5% of standard deviation).
 336

337 4.2 Sensitivity of the SWI metrics

338 The Sobol' indices for the concentration at the observation points (A1, A2, A3) as well as for
 339 the SWI metrics are depicted in Table 5. This table also gives the mean value and the standard
 340 deviation for all quantities of interest.

341 **Table 5.** Sensitivity of the concentration at the observation points (A1, A2 and A3) and of
 342 the SWI metrics. S_1 , S_2 and S_3 represent the first order Sobol' indices for the sensitivity to

343 α_L^0 , α_T^0 and ℓ_0 . ‘mean’ and ‘std’ represent the mean value and the standard deviation for the
 344 quantities of interest.

345

	mean	std	S_1	S_2	S_3	$\sum_{i=1}^3 S_i$
A1	0.17	0.12	0.01	0.81	0.04	0.86
A2	0.79	0.1	0.27	0.24	0.42	0.94
A3	0.27	0.11	0.02	0.33	0.6	0.95
$X_{0.1}$	1.39	0.17	0.13	0.64	0.06	0.82
$X_{0.5}$	2.0	0.19	0.07	0.73	0.13	0.93
$X_{0.9}$	2.66	0.19	0.30	0.16	0.46	0.93
L_S	1.27	0.23	0.5	0.05	0.41	0.97
Total mass	1016	110	0.16	0.16	0.35	0.67

346

347 The results of this table show that

348 - The concentration near A1 is mostly influenced by α_T^0 ($S_2 = 0.81$). In this region,

349 moderate interactions occur between parameters $\left(\sum_{i=1}^3 S_i = 0.86\right)$. The effects of α_L^0 and

350 ℓ_0 alone are insignificant ($S_2 = 0.01$ and $S_3 = 0.04$), but their total effects (including

351 interactions) are moderately significant ($ST_1 = 0.12$ and $ST_3 = 0.11$). The results around

352 A1 are coherent with the results discussed previously based on the spatial maps of

353 Sobol’ indices (Figure 4).

354 - Around A2, located near the sea boundary, high concentrations can be observed

355 (mean=0.79). The concentration has slight variability (std=0.1) which indicates that

356 SWI reaches this point whatever the values of the dispersion parameters. The most

357 influential parameter near A2 is ℓ_0 ($S_3 = 0.42$). The parameters α_L^0 and α_T^0 have

358 significant and close effects ($S_1 = 0.27$ and $S_2 = 0.24$). Interactions between dispersion

359 parameters are not significant $\left(\sum_{i=1}^3 S_i = 0.94 \right)$.

360 - The point A3 is located near the top of the domain and close to the sea boundary. The
361 standard deviation (std=0.11) of concentrations is relatively significant (mean=0.27).

362 The most influential parameter in this region is ℓ_0 ($S_3 = 0.6$) followed by the parameter
363 α_T^0 ($S_2 = 0.33$). The parameter α_L^0 is irrelevant ($S_1 = 0.02$). Interactions between the

364 three dispersion parameters are not significant $\left(\sum_{i=1}^3 S_i = 0.95 \right)$.

365 - The 10% isochlor intersects the substratum at an average distance of 1.39 m from the
366 sea boundary. $X_{0.1}$ has high variability (std=0.17m). The parameter α_T^0 is the most

367 influential parameter ($S_2 = 0.64$). The parameter α_L^0 has a small first order sensitivity
368 index ($S_1 = 0.13$) whereas the parameter ℓ_0 has a negligible first order sensitivity index

369 ($S_3 = 0.06$). However, because of interaction between parameters $\left(\sum_{i=1}^3 S_i = 0.82 \right)$, α_L^0

370 and ℓ_0 are influential since their total sensitivity indices are significant ($ST_1 = 0.29$ and
371 $ST_2 = 0.2$).

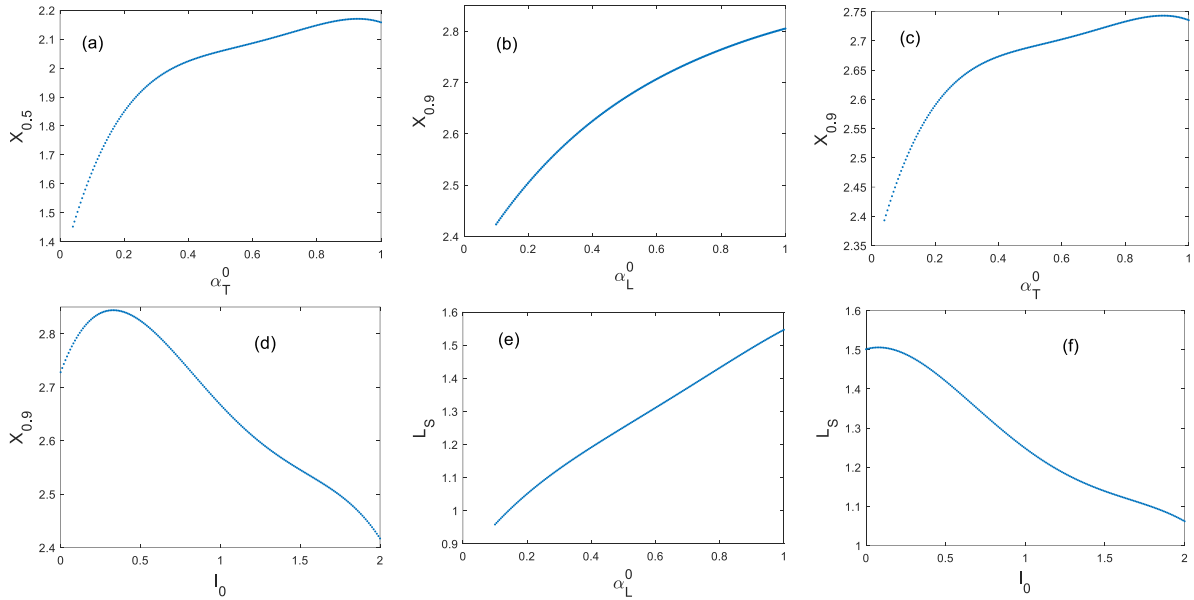
372 - The 50% isochlor intersects the substratum at an average distance of 2.0 m. The
373 dispersion parameters have a strong effect on that position since the standard deviation

374 is significant (std=0.19). As $X_{0.1}$, $X_{0.5}$ is mainly controlled by the parameter α_T^0
375 ($S_2 = 0.73$). The parameters α_L^0 ($S_1 = 0.07$) and ℓ_0 ($S_3 = 0.13$) have a limited effect.

376 Because the 50% isochlor is closer to the sea than the 10% isochlor, $X_{0.5}$ is more

377 sensitive to ℓ_0 than $X_{0.1}$. Small interactions are observed between the dispersion

378 parameters $\left(\sum_{i=1}^3 S_i = 0.93\right)$. Therefore, $X_{0.5}$ and in consequence L_{toe} are mainly
 379 controlled by the asymptotic transverse dispersivity. Since interactions are small, the
 380 marginal effect of α_T^0 , depicted in the Figure 5a, reflects the behavior of $X_{0.5}$ when
 381 varying α_T^0 (the other parameters are set at their mean values). Figure 5a shows a high
 382 sensitivity for $\alpha_T^0 \leq 0.3$ and a weaker sensitivity for higher values of α_T^0 . In this figure,
 383 $X_{0.5}$ increases with α_T^0 which is consistent with physics as the decrease in α_T^0 induces
 384 more saltwater intrusion and hence a decrease of $X_{0.5}$.



385 **Figure 5.** Marginal effect of: (a) α_T^0 on $X_{0.5}$, (b) α_L^0 on $X_{0.9}$, (c) α_T^0 on $X_{0.9}$, (d) l_0 on
 386 $X_{0.9}$, (e) α_L^0 on L_s and (f) l_0 on L_s
 387

388 - The 90% isochlor intersects the substratum at an average distance of 2.66 m with a
 389 standard deviation of 0.19 m. $X_{0.9}$ is sensitive to the three dispersion parameters. As the
 390 isochlor 90% is close to the sea, the most influential parameter is l_0 ($S_3 = 0.46$), comes
 391 next α_L^0 ($S_1 = 0.30$) and finally α_T^0 ($S_2 = 0.16$). Small interactions exist between the

392 dispersion parameters $\left(\sum_{i=1}^3 S_i = 0.93\right)$. Marginal effects of the three sensitive dispersion
393 parameters on $X_{0.9}$ are plotted in the Figure 5. The sensitivity of $X_{0.9}$ to α_L^0 (Figure 5b)
394 has a positive slope as an increase of α_L^0 induces an increase of the spreading of the
395 concentration front resulting in an increase of $X_{0.9}$. The sensitivity of $X_{0.9}$ to α_T^0 (Figure
396 5c) is similar to that observed for $X_{0.5}$. This demonstrates that saltwater intrusion is
397 mainly controlled by the asymptotic transverse dispersivity. A decrease of α_T^0 induces
398 more intrusion which results in a decrease of $X_{0.5}$ and $X_{0.9}$. The sensitivity of the
399 intrusion to α_T^0 is more pronounced for small values of this parameter. The $X_{0.9}$ varies
400 almost linearly with a negative slope with respect to the parameter ℓ_0 (Figure 5d).
401 Indeed, the 90% isochlor is located near the sea boundary (the average $X_{0.9}$ is 2.66m)
402 where the effect of ℓ_0 is significant (see Figure 4c). In that region, the increase of ℓ_0
403 yields less dispersion effects which results in more saltwater intrusion and hence a
404 decrease in $X_{0.9}$.

405 - For the spread of the concentration (L_S), the most influential parameter is α_L^0 ($S_1 = 0.5$)
406 , followed by ℓ_0 ($S_3 = 0.41$). The sensitivity of L_S to α_L^0 is much more important than
407 that of $X_{0.1}$ and $X_{0.9}$. Furthermore, although α_T^0 is influential on $X_{0.9}$ and on $X_{0.1}$, it
408 has no effect on L_S ($S_2 = 0.05$). The interactions between parameters are almost absent
409 $\left(\sum_{i=1}^3 S_i = 0.97\right)$. The marginal effects of the parameters α_L^0 and ℓ_0 on L_S are depicted
410 in the Figure 5. L_S increases linearly with the value of α_L^0 (Figure 5e). This confirms
411 that the spreading is directly proportional to the value of α_L^0 . The sensitivity of L_S to

412 ℓ_0 has a negative slope (Figure 5f). The increase of ℓ_0 yields less dispersion which
413 results in less spreading of the concentration front and hence a reduction in L_S .

414 - The standard deviation of the total mass in the aquifer is around 10% of its mean value.
415 Significant interactions occur between the dispersion parameters $\left(\sum_{i=1}^3 S_i = 0.67\right)$. The
416 total sensitivity indices of the three dispersion parameters ($ST_1 = 0.46$, $ST_2 = 0.23$ and
417 $ST_3 = 0.64$) are significantly higher than their first order indices ($S_1 = 0.16$, $S_2 = 0.16$
418 and $S_3 = 0.35$). This shows that ℓ_0 plays the most important role on the amount of mass
419 which has intruded into the domain, followed by α_L^0 . Strong interactions mainly occur
420 between these two parameters since $ST_3 - S_3 = 0.29$ and $ST_1 - S_1 = 0.3$ whereas
421 $ST_2 - S_2 = 0.07$.

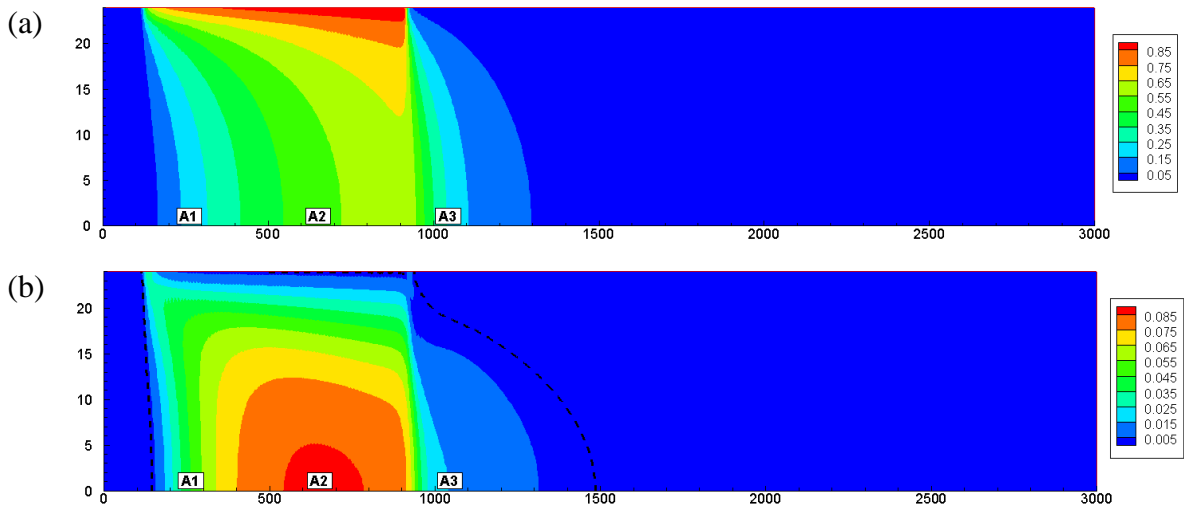
422 **5. Results of the leachate transport problem**

423 Starting with no leachate in the aquifer, the leachate transport problem is simulated for 24 years.
424 A mesh converged solution is obtained using a uniform triangular mesh formed by 14400
425 triangular elements. A hundred simulations were performed using independent random
426 parameter values generated inside the intervals given in Table 4. The mean leachate plume is
427 shown in the Figure 6a. The leachate enters the aquifer due to dispersion and vertical infiltration.
428 Within the aquifer, the leachate plume moves to the right side due to the hydraulic gradient
429 between left and right sides. A stable flow is obtained for all explored dispersivity values
430 because of (i) the large dispersion and (ii) the weak density difference between the contaminant
431 and freshwater.

432

433

434



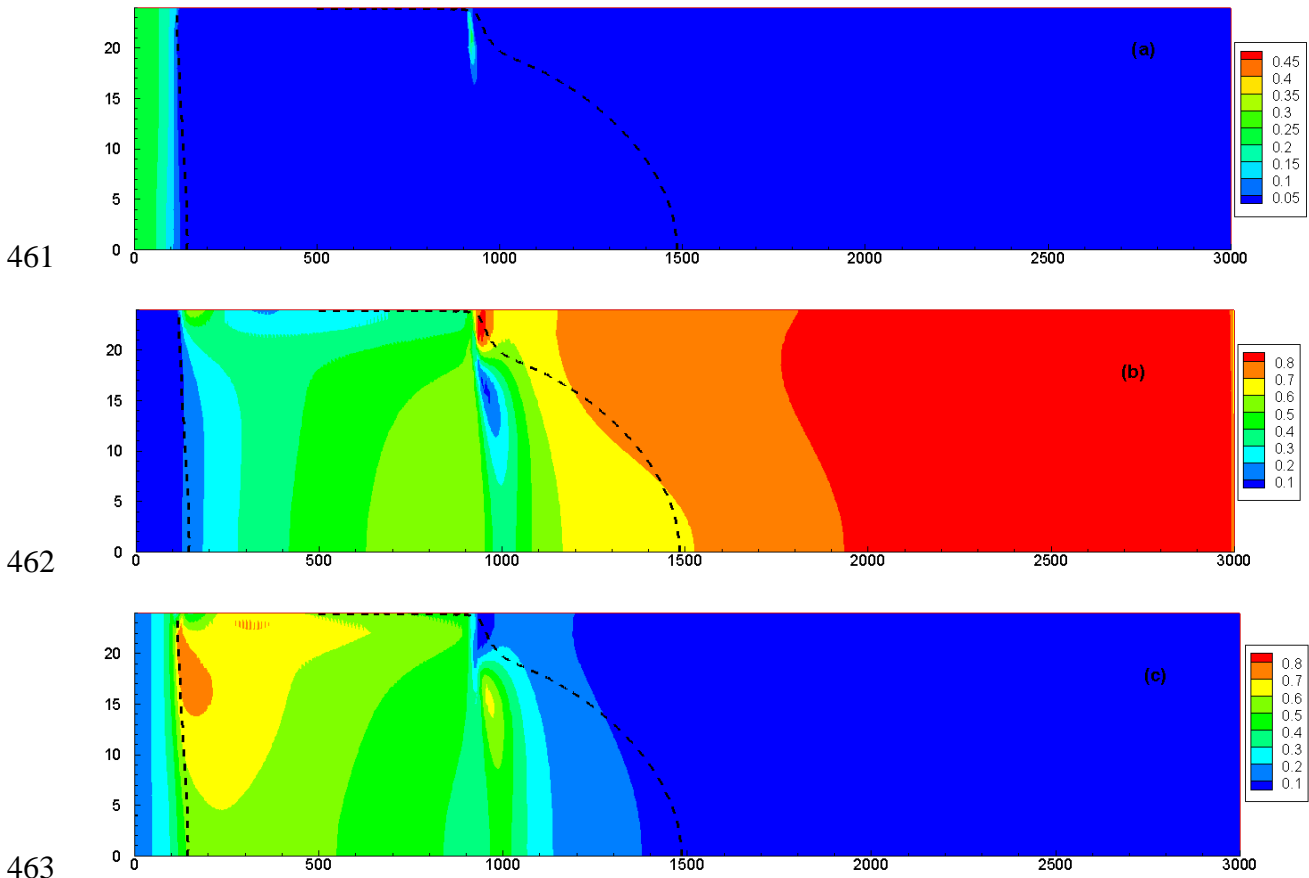
435

436 **Figure 6.** The leachate transport problem at 24 years: (a) Spatial map of the mean concentration
 437 values and (b) Spatial map of variance of concentration. The dashed contour delimits the region
 438 of high variances (5% of standard deviation).
 439

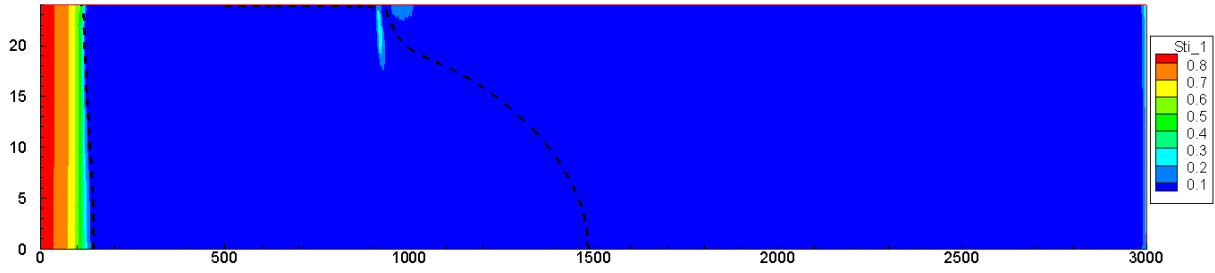
440 The distribution of the variance of the concentration shows that high variability is located below
 441 the disposal site (Figure 6b) towards the bottom of the aquifer. The center of the zone of high
 442 variability is shifted to the right of the disposal site center because of the basic advective flow
 443 in the aquifer which goes from left to right.

444 Figure 7 shows the spatial distributions of the first-order Sobol' indices. For the region of
 445 significant variability (delimited by dashed lines), the asymptotic longitudinal dispersivity α_L^0
 446 has a negligible first-order sensitivity index (Figure 7a). Note that this does not imply the
 447 irrelevance of α_L^0 since the first-order index does not take into account interactions between
 448 parameters. To judge the inefficiency of α_L^0 , we evaluate the total Sobol index of α_L^0 . Figure
 449 8 shows that, in the region of high variance, α_L^0 has no effect on the concentration distribution
 450 (neither alone nor in interaction with the other parameters). Therefore, the parameter α_L^0 is
 451 irrelevant for concentration distribution. Thus, in this case, mixing by dispersion is mainly
 452 related to transverse dispersivity. The parameters α_T^0 and ℓ_0 have strong influence on the
 453 concentration distribution (Figure 7b and 7c) in the region of high variability (below the landfill

454 site). Significant interactions are observed between these two parameters. The amount of
 455 interaction between parameters can be evaluated by computing $r = 1 - \sum_i S_i$. If interactions
 456 between parameters are absent, then $\sum_i S_i = 1$ and $r = 0$. Figure 9 shows that interactions
 457 between α_T^0 and ℓ_0 are observed in two regions located in the lower half of domain. Moderate
 458 interactions occur in the region between $x = 100$ m and $x = 500$ m. Higher interactions occur in
 459 a larger zone located downstream the deposit site between $x = 1000$ m and $x = 1500$ m.
 460

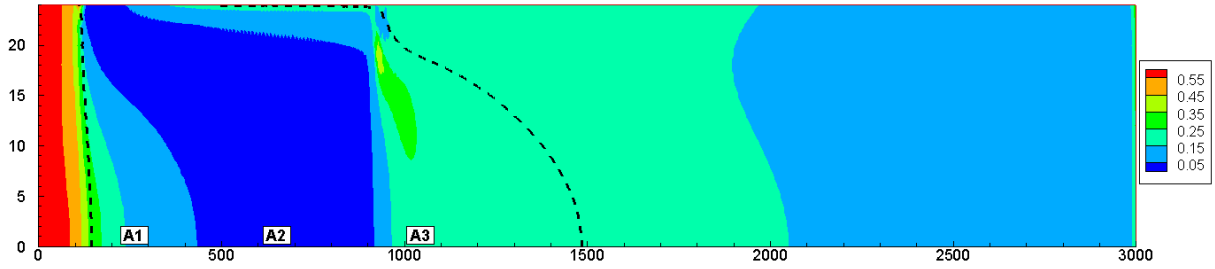


464 **Figure 7.** Spatial map of the first order sensitivity indices for the leachate transport problem:
 465 a) sensitivity to α_L^0 , b) sensitivity to α_T^0 and c) sensitivity to ℓ_0 .



466

467 **Figure 8.** Spatial map of the total Sobol' index of α_L^0 for the leachate transport problem.



468

469 **Figure 9.** Spatial map of the interaction $r = 1 - \sum_i S_i$ for the leachate transport problem.

470

471 The effects of dispersion parameters are investigated for the total mass in the domain and for
 472 the final concentration at the following selected points A_1 (265,0); A_2 (655,0) and A_3 (1025,0)
 473 in Table 6. The results of this table show that:

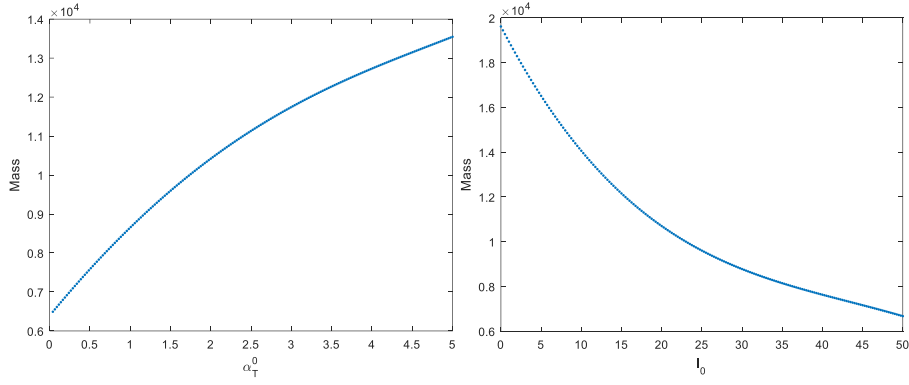
474

	mean	std	S_1	S_2	S_3	$\sum_{i=1}^3 S_i$
A1	0.19	0.2	0.0	0.29	0.58	0.87
A2	0.52	0.3	0.	0.51	0.46	0.97
A3	0.29	0.13	0.0	0.37	0.39	0.76
Total mass	10667	4058	0.0	0.24	0.74	0.98

475

476 **Table 6.** Sobol's indices for the concentration at the observation points ($A_{1,...,3}$) and for the
 477 total mass in the domain for the leachate transport problem. S_1 , S_2 and S_3 represent the first
 478 order Sobol' indices for the sensitivity to α_L^0 , α_T^0 and ℓ_0 . 'mean' and 'std' represent the
 479 mean value and the standard variation for the quantities of interest.

- 480 - The concentration around A1 is first influenced by ℓ_0 ($S_3 = 0.58$) and then by α_T^0
481 ($S_2 = 0.29$). The parameter α_L^0 is irrelevant ($ST_1 = 0$). Moderate interactions occur
482 between α_L^0 and ℓ_0 $\left(\sum_{i=1}^3 S_i = 0.87\right)$.
- 483 - The concentration around A2 is almost equally influenced by α_T^0 ($S_2 = 0.51$) and ℓ_0
484 ($S_3 = 0.46$). In this region, the model is almost additive since interactions between
485 parameters are almost absent $\left(\sum_{i=1}^3 S_i = 0.97\right)$.
- 486 - Around A3, the parameters α_T^0 and ℓ_0 have close first-order sensitivity indices
487 ($S_2 = 0.37$ and $S_3 = 0.39$) and close total sensitivity indices ($ST_2 = 0.6$ and
488 $ST_3 = 0.63$). In this region, strong interactions occur between these two parameters
489 $\left(\sum_{i=1}^3 S_i = 0.76\right)$.
- 490 - The total mass in the system has a mean of 10,667 and a significant variance of 4,058.
491 The parameter α_L^0 has no effect ($S_1 = 0$). The parameter ℓ_0 has a strong effect on the
492 total mass value. This effect ($S_3 = 0.74$) is three times more important than the effect
493 of α_T^0 ($S_2 = 0.24$). The effects of the two parameters are additive since interactions
494 between them are almost absent $\left(\sum_{i=1}^3 S_i = 0.98\right)$. The marginal effects of the parameters
495 α_T^0 and ℓ_0 on the total mass are plotted in Figure 10. The sensitivity of the total mass
496 to α_T^0 depicts a curve with a positive slope since the total mass increases as α_T^0
497 increases. The marginal effect of ℓ_0 is represented by a negative slope curve which is
498 consistent with physics. The leachate plume, and consequently the total mass, increase
499 as dispersion increases (*i.e.* ℓ_0 decreases).



500

501

502

Figure 10. Marginal effects of α_T^0 , and ℓ_0 on the total mass for the leachate transport problem.

503 **6. Conclusions**

504

505

506

507

508

509

510

511

512

513

514

515

516

517

518

519

Transport of pollutants in aquifers is usually modeled using the advection-dispersion transport equation with constant-dispersion coefficients. Recently, laboratory and field transport observations have shown that dispersivities are distance-dependent. The most popular function for distance-dependent dispersivity is the linear-asymptotic model which assumes that the longitudinal and transverse dispersion coefficients increase linearly with the distance from the source of contamination until some asymptotic distance ℓ_0 , after which the dispersion coefficients reach asymptotic values. In the literature, this model has been investigated in simple configurations dealing with either one-dimensional or uniform two-dimensional flow fields. In this work, we investigate the effects of asymptotic dispersion model in the case of contaminant transport with DDF that involves complex velocity field. The linear-asymptotic model has been incorporated in an advanced in-house DDF numerical model. The new developed code was used to investigate the effect of the dispersion coefficients (asymptotic longitudinal dispersivity α_L^0 , asymptotic transverse dispersivity α_T^0 and asymptotic distance ℓ_0) on the contamination plume for two conceptual models: the Henry saltwater intrusion problem and a leachate transport problem from a surface deposit site. The effects of dispersion parameters are evaluated using Global Sensitivity Analysis (GSA) combined with the

520 Polynomial Chaos Expansion (PCE) surrogate modelling to compute both first-order and total
521 Sobol' sensitivity indices

522 The results for the Henry problem showed that the concentration at the center bottom of the
523 domain, is mostly influenced by the asymptotic value of the transverse dispersion α_T^0 whereas,
524 near the sea boundary, the most influential parameter is the asymptotic distance ℓ_0 . The
525 position of the 50% isochlor is mainly controlled by the parameter α_T^0 . The spread of the
526 concentration is not influenced by α_T^0 but by α_L^0 and ℓ_0 . The total amount of mass intruded in
527 the aquifer is influenced by ℓ_0 and then by α_L^0 and interactions between them.

528 The results for the leachate transport problem show that α_L^0 has no effect (neither alone nor in
529 interaction with the other parameters) on the concentration distribution. The parameters α_T^0
530 and ℓ_0 have a strong influence on the concentration distribution below the landfill site. Strong
531 interactions occur between these two parameters in the aquifer. The total mass in the aquifer is
532 strongly influenced by ℓ_0 . The sensitivity to ℓ_0 is three times more important than to α_T^0 and
533 the effects of these two parameters on the total mass are additive (interactions are insignificant).

534 This study showed that distance-dependent dispersion coefficients can significantly affect
535 contaminant distribution in aquifers in the case of density-driven flow. It demonstrates the
536 advantage of using GSA with PCE surrogate modeling for such investigation since it allows to
537 determine, for each parameter, the regions of high influence and the regions where the effect of
538 the parameter is insignificant. It also allows to determine regions of high interactions between
539 parameters and to explore the marginal effect of sensitive parameters on the model output.

540
541
542
543

544 **Acknowledgments**

545 This work was partially supported by the Tunisian-French joint international laboratory NAILA
546 (<http://www.lmi-naila.com/>). Marwan Fahs would acknowledge the support from the national
547 school of water and environmental engineering of Strasbourg through the research project
548 PORO6100. Behzad Ataie-Ashtiani and Craig T. Simmons acknowledge support from the
549 National Centre for Groundwater Research and Training, Australia. Behzad Ataie-Ashtiani also
550 appreciates the support of the Research Office of the Sharif University of Technology, Iran.
551 The data used in this work are available on the GitHub repository: <https://github.com/fahs->

552 LHYGES

553

- 555 1. Abarca, E., Carrera, J., Sánchez-Vila, X., & Dentz, M. (2007). Anisotropic dispersive Henry
 556 problem. *Advances in Water Resources*, 30(4), 913–926.
 557 <https://doi.org/10.1016/j.advwatres.2006.08.005>
- 558 2. Ackerer, P., & Younes, A. (2008). Efficient approximations for the simulation of density
 559 driven flow in porous media. *Advances in Water Resources*, 31(1), 15–27.
 560 <https://doi.org/10.1016/j.advwatres.2007.06.001>
- 561 3. Basha, H. A., & El-Habel, F. S. (1993). Analytical solution of the one-dimensional time-
 562 dependent transport equation. *Water Resources Research*, 29(9), 3209–3214.
 563 <https://doi.org/10.1029/93WR01038>
- 564 4. Berkowitz, B., Scher, H., Silliman, S.E., 2000. Anomalous transport in laboratory-scale,
 565 heterogeneous porous media. *Water Resour. Res.* 36, 149–158.
 566 <https://doi.org/10.1029/1999WR900295>
- 567 5. Chen, J.-S., Liu, C.-W., Hsu, H.-T., & Liao, C.-M. (2003). A Laplace transform power
 568 series solution for solute transport in a convergent flow field with scale-dependent
 569 dispersion. *Water Resources Research*, 39(8). <https://doi.org/10.1029/2003WR002299>
- 570 6. Chen, J.-S., Liu, C.-W., & Liang, C.-P. (2006). Evaluation of longitudinal and transverse
 571 dispersivities/distance ratios for tracer test in a radially convergent flow field with scale-
 572 dependent dispersion. *Advances in Water Resources*, 29(6), 887–898.
 573 <https://doi.org/10.1016/j.advwatres.2005.08.001>
- 574 7. Chen, J.-S., Chen, C.-S., & Chen, C. Y. (2007). Analysis of solute transport in a divergent
 575 flow tracer test with scale-dependent dispersion. *Hydrological Processes*, 21(18), 2526–
 576 2536. <https://doi.org/10.1002/hyp.6496>
- 577 8. Chen, J.-S., Ni, C.-F., Liang, C.-P., & Chiang, C.-C. (2008a). Analytical power series
 578 solution for contaminant transport with hyperbolic asymptotic distance-dependent
 579 dispersivity. *Journal of Hydrology*, 362(1–2), 142–149.
 580 <https://doi.org/10.1016/j.jhydrol.2008.08.020>
- 581 9. Chen, J.-S., Ni, C.-F., & Liang, C.-P. (2008b). Analytical power series solutions to the two-
 582 dimensional advection-dispersion equation with distance-dependent dispersivities.
 583 *Hydrological Processes*, 22(24), 4670–4678. <https://doi.org/10.1002/hyp.7067>
- 584 10. Cortis, A., & Berkowitz, B. (2004). Anomalous Transport in “Classical” Soil and Sand
 585 Columns. *Soil Science Society of America Journal*, 68(5), 1539–1548.
 586 <https://doi.org/10.2136/sssaj2004.1539>
- 587 11. Dai, Z., Zhan, C., Dong, S., Yin, S., Zhang, X., & Soltanian, M. R. (2020). How does
 588 resolution of sedimentary architecture data affect plume dispersion in multiscale and
 589 hierarchical systems? *Journal of Hydrology*, 582, 124516.
 590 <https://doi.org/10.1016/j.jhydrol.2019.124516>
- 591 12. David Logan, J. (1996). Solute transport in porous media with scale-dependent dispersion
 592 and periodic boundary conditions. *Journal of Hydrology*, 184(3–4), 261–276.
 593 [https://doi.org/10.1016/0022-1694\(95\)02976-1](https://doi.org/10.1016/0022-1694(95)02976-1)
- 594 13. Dentz, M., Cortis, A., Scher, H., Berkowitz, B., 2004. Time behavior of solute transport in
 595 heterogeneous media: transition from anomalous to normal transport. *Advances in Water*
 596 *Resources* 27, 155–173. <https://doi.org/10.1016/j.advwatres.2003.11.002>
- 597 14. Emami-Meybodi, H. (2017). Dispersion-driven instability of mixed convective flow in
 598 porous media. *Physics of Fluids*, 29(9), 094102. <https://doi.org/10.1063/1.4990386>
- 599 15. Fahs, M., Ataie-Ashtiani, B., Younes, A., Simmons, C. T., & Ackerer, P. (2016). The Henry
 600 problem: New semianalytical solution for velocity-dependent dispersion. *Water Resources*
 601 *Research*, 52(9), 7382–7407. <https://doi.org/10.1002/2016WR019288>
- 602 16. Fahs, M., Koohbor, B., Belfort, B., Ataie-Ashtiani, B., Simmons, C., Younes, A., &

- 603 Ackerer, P. (2018). A Generalized Semi-Analytical Solution for the Dispersive Henry
604 Problem: Effect of Stratification and Anisotropy on Seawater Intrusion. *Water*, 10(2), 230.
605 <https://doi.org/10.3390/w10020230>
- 606 17. Fahs, M., Graf, T., Tran, T. V., Ataie-Ashtiani, B., Simmons, Craig. T., & Younes, A.
607 (2020). Study of the Effect of Thermal Dispersion on Internal Natural Convection in Porous
608 Media Using Fourier Series. *Transport in Porous Media*, 131(2), 537–568.
609 <https://doi.org/10.1007/s11242-019-01356-1>
- 610 18. Fajraoui, N., Mara, T. A., Younes, A., & Bouhlila, R. (2012). Reactive Transport Parameter
611 Estimation and Global Sensitivity Analysis Using Sparse Polynomial Chaos Expansion.
612 *Water, Air, & Soil Pollution*, 223(7), 4183–4197. <https://doi.org/10.1007/s11270-012-1183-8>
- 614 19. Fajraoui, Noura, Fahs, M., Younes, A., & Sudret, B. (2017). Analyzing natural convection
615 in porous enclosure with polynomial chaos expansions: Effect of thermal dispersion,
616 anisotropic permeability and heterogeneity. *International Journal of Heat and Mass
617 Transfer*, 115, 205–224. <https://doi.org/10.1016/j.ijheatmasstransfer.2017.07.003>
- 618 20. Frind, E. O. (1982). Simulation of long-term transient density-dependent transport in
619 groundwater. *Advances in Water Resources*, 5(2), 73–88. [https://doi.org/10.1016/0309-1708\(82\)90049-5](https://doi.org/10.1016/0309-1708(82)90049-5)
- 621 21. Gao, G., Zhan, H., Feng, S., Fu, B., Ma, Y., & Huang, G. (2010). A new mobile-immobile
622 model for reactive solute transport with scale-dependent dispersion. *Water Resources
623 Research*, 46(8). <https://doi.org/10.1029/2009WR008707>
- 624 22. Gao, G., Zhan, H., Feng, S., Fu, B., & Huang, G. (2012). A mobile-immobile model with
625 an asymptotic scale-dependent dispersion function. *Journal of Hydrology*, 424–425, 172–
626 183. <https://doi.org/10.1016/j.jhydrol.2011.12.041>
- 627 23. Gelhar, L. W., Welty, C., & Rehfeldt, K. R. (1992). A critical review of data on field-scale
628 dispersion in aquifers. *Water Resources Research*, 28(7), 1955–1974.
629 <https://doi.org/10.1029/92WR00607>
- 630 24. Guevara Morel, C. R., van Reeuwijk, M., & Graf, T. (2015). Systematic investigation of
631 non-Boussinesq effects in variable-density groundwater flow simulations. *Journal of
632 Contaminant Hydrology*, 183, 82–98. <https://doi.org/10.1016/j.jconhyd.2015.10.004>
- 633 25. Henry, H. R. (1964). Effects of dispersion on salt encroachment in coastal aquifers, 1613–
634 C, 70–84.
- 635 26. Huang, G., Huang, Q., & Zhan, H. (2006). Evidence of one-dimensional scale-dependent
636 fractional advection–dispersion. *Journal of Contaminant Hydrology*, 85(1–2), 53–71.
637 <https://doi.org/10.1016/j.jconhyd.2005.12.007>
- 638 27. Huang, K., Toride, N., & Van Genuchten, M. Th. (1995). Experimental investigation of
639 solute transport in large, homogeneous and heterogeneous, saturated soil columns.
640 *Transport in Porous Media*, 18(3), 283–302. <https://doi.org/10.1007/BF00616936>
- 641 28. Hunt, B. (2002). Scale-Dependent Dispersion from a Pit. *Journal of Hydrologic
642 Engineering*, 7(2), 168–174. [https://doi.org/10.1061/\(ASCE\)1084-0699\(2002\)7:2\(168\)](https://doi.org/10.1061/(ASCE)1084-0699(2002)7:2(168))
- 643 29. Kangle, H., van Genuchten, M. T., & Renduo, Z. (1996). Exact solutions for one-
644 dimensional transport with asymptotic scale-dependent dispersion. *Applied Mathematical
645 Modelling*, 20(4), 298–308. [https://doi.org/10.1016/0307-904X\(95\)00123-2](https://doi.org/10.1016/0307-904X(95)00123-2)
- 646 30. Kerrou, J., Renard, P., 2010. A numerical analysis of dimensionality and heterogeneity
647 effects on advective dispersive seawater intrusion processes. *Hydrogeol J* 18, 55–72.
648 <https://doi.org/10.1007/s10040-009-0533-0>
- 649 31. Khan, A. U.-H., & Jury, W. A. (1990). A laboratory study of the dispersion scale effect in
650 column outflow experiments. *Journal of Contaminant Hydrology*, 5(2), 119–131.
651 [https://doi.org/10.1016/0169-7722\(90\)90001-W](https://doi.org/10.1016/0169-7722(90)90001-W)
- 652 32. Kitanidis, P. K. (2017). Teaching and communicating dispersion in hydrogeology, with

- 653 emphasis on the applicability of the Fickian model. *Advances in Water Resources*, 106, 11–
654 23. <https://doi.org/10.1016/j.advwatres.2017.01.006>
- 655 33. Liu, Y., & Kitanidis, P. K. (2013). A mathematical and computational study of the
656 dispersivity tensor in anisotropic porous media. *Advances in Water Resources*, 62, 303–
657 316. <https://doi.org/10.1016/j.advwatres.2013.07.015>
- 658 34. Mara, T. A., Belfort, B., Fontaine, V., & Younes, A. (2017). Addressing factors fixing
659 setting from given data: A comparison of different methods. *Environmental Modelling &*
660 *Software*, 87, 29–38. <https://doi.org/10.1016/j.envsoft.2016.10.004>
- 661 35. Mishra, S., & Parker, J. C. (1990). Analysis of solute transport with a hyperbolic scale-
662 dependent dispersion model. *Hydrological Processes*, 4(1), 45–57.
663 <https://doi.org/10.1002/hyp.3360040105>
- 664 36. Molz, F. J., Guven, O., & Melville, J. G. (1983). An Examination of Scale-Dependent
665 Dispersion Coefficients. *Ground Water*, 21(6), 715–725. <https://doi.org/10.1111/j.1745-6584.1983.tb01942.x>
- 666 37. Pang, L., & Hunt, B. (2001). Solutions and verification of a scale-dependent dispersion
667 model. *Journal of Contaminant Hydrology*, 53(1–2), 21–39. [https://doi.org/10.1016/S0169-7722\(01\)00134-6](https://doi.org/10.1016/S0169-7722(01)00134-6)
- 668 38. Pérez Guerrero, J. S., & Skaggs, T. H. (2010). Analytical solution for one-dimensional
669 advection–dispersion transport equation with distance-dependent coefficients. *Journal of*
670 *Hydrology*, 390(1–2), 57–65. <https://doi.org/10.1016/j.jhydrol.2010.06.030>
- 671 39. Pickens, J. F., & Grisak, G. E. (1981a). Modeling of scale-dependent dispersion in
672 hydrogeologic systems. *Water Resources Research*, 17(6), 1701–1711.
673 <https://doi.org/10.1029/WR017i006p01701>
- 674 40. Pickens, J. F., & Grisak, G. E. (1981b). Scale-dependent dispersion in a stratified granular
675 aquifer. *Water Resources Research*, 17(4), 1191–1211.
676 <https://doi.org/10.1029/WR017i004p01191>
- 677 41. Pool, M., Post, V.E.A., Simmons, C.T., 2015. Effects of tidal fluctuations and spatial
678 heterogeneity on mixing and spreading in spatially heterogeneous coastal aquifers. *Water*
679 *Resour. Res.* 51, 1570–1585. <https://doi.org/10.1002/2014WR016068>
- 680 42. Saltelli, A., Ratto, M., Tarantola, S., & Campolongo, F. (2006). Sensitivity analysis
681 practices: Strategies for model-based inference. *Reliability Engineering & System Safety*,
682 91(10–11), 1109–1125. <https://doi.org/10.1016/j.ress.2005.11.014>
- 683 43. Schulze-Makuch, D. (2005). Longitudinal dispersivity data and implications for scaling
684 behavior. *Ground Water*, 43(3), 443–456. <https://doi.org/10.1111/j.1745-6584.2005.0051.x>
- 685 44. Shao, Q., Younes, A., Fahs, M., & Mara, T. A. (2017). Bayesian sparse polynomial chaos
686 expansion for global sensitivity analysis. *Computer Methods in Applied Mechanics and*
687 *Engineering*, 318, 474–496. <https://doi.org/10.1016/j.cma.2017.01.033>
- 688 45. Shao, Q., Fahs, M., Hoteit, H., Carrera, J., Ackerer, P., & Younes, A. (2018). A 3-D
689 Semianalytical Solution for Density-Driven Flow in Porous Media. *Water Resources*
690 *Research*, 54(12). <https://doi.org/10.1029/2018WR023583>
- 691 46. Sharma, P. K., & Abgaze, T. A. (2015). Solute transport through porous media using
692 asymptotic dispersivity. *Sadhana*, 40(5), 1595–1609. <https://doi.org/10.1007/s12046-015-0382-6>
- 693 47. Silliman, S. E., & Simpson, E. S. (1987). Laboratory evidence of the scale effect in
694 dispersion of solutes in porous media. *Water Resources Research*, 23(8), 1667–1673.
695 <https://doi.org/10.1029/WR023i008p01667>
- 696 48. Simpson, M. J., & Clement, T. P. (2004). Improving the worthiness of the Henry problem
697 as a benchmark for density-dependent groundwater flow models. *Water Resources*
698 *Research*, 40(1). <https://doi.org/10.1029/2003WR002199>
- 699 49. Sobol', I. M. (2001). Global sensitivity indices for nonlinear mathematical models and their
700
701
702

- 703 Monte Carlo estimates. *Mathematics and Computers in Simulation*, 55(1–3), 271–280.
 704 [https://doi.org/10.1016/S0378-4754\(00\)00270-6](https://doi.org/10.1016/S0378-4754(00)00270-6)
- 705 50. Sudret, B. (2008). Global sensitivity analysis using polynomial chaos expansions.
 706 *Reliability Engineering & System Safety*, 93(7), 964–979.
 707 <https://doi.org/10.1016/j.ress.2007.04.002>
- 708 51. Vanderborght, J., & Vereecken, H. (2007). Review of Dispersivities for Transport Modeling
 709 in Soils. *Vadose Zone Journal*, 6(1), 29–52. <https://doi.org/10.2136/vzj2006.0096>
- 710 52. Wang, H., Persaud, N., Zhou, X., 2006. Specifying Scale-dependent Dispersivity in
 711 Numerical Solutions of the Convection-Dispersion Equation. *Soil Sci. Soc. Am. J.* 70,
 712 1843–1850. <https://doi.org/10.2136/sssaj2005.0166>
- 713 53. Wang, Q., Gu, H., Zhan, H., Shi, W., & Zhou, R. (2019). Mixing Effect on Reactive
 714 Transport in a Column with Scale Dependent Dispersion. *Journal of Hydrology*, 124494.
 715 <https://doi.org/10.1016/j.jhydrol.2019.124494>
- 716 54. Wen, B., Chang, K. W., & Hesse, M. A. (2018). Rayleigh-Darcy convection with
 717 hydrodynamic dispersion. *Physical Review Fluids*, 3(12), 123801.
 718 <https://doi.org/10.1103/PhysRevFluids.3.123801>
- 719 55. Werner, A. D., Bakker, M., Post, V. E. A., Vandenbohede, A., Lu, C., Ataie-Ashtiani, B.,
 720 et al. (2013). Seawater intrusion processes, investigation and management: Recent advances
 721 and future challenges. *Advances in Water Resources*, 51, 3–26.
 722 <https://doi.org/10.1016/j.advwatres.2012.03.004>
- 723 56. Wheatcraft, S. W., & Tyler, S. W. (1988). An explanation of scale-dependent dispersivity
 724 in heterogeneous aquifers using concepts of fractal geometry. *Water Resources Research*,
 725 24(4), 566–578. <https://doi.org/10.1029/WR024i004p00566>
- 726 57. Yates, S. R. (1992). An analytical solution for one-dimensional transport in porous media
 727 with an exponential dispersion function. *Water Resources Research*, 28(8), 2149–2154.
 728 <https://doi.org/10.1029/92WR01006>
- 729 58. You, K., & Zhan, H. (2013). New solutions for solute transport in a finite column with
 730 distance-dependent dispersivities and time-dependent solute sources. *Journal of Hydrology*,
 731 487, 87–97. <https://doi.org/10.1016/j.jhydrol.2013.02.027>
- 732 59. Younes, A., Delay, F., Fajraoui, N., Fahs, M., & Mara, T. A. (2016). Global sensitivity
 733 analysis and Bayesian parameter inference for solute transport in porous media colonized
 734 by biofilms. *Journal of Contaminant Hydrology*, 191, 1–18.
 735 <https://doi.org/10.1016/j.jconhyd.2016.04.007>
- 736 60. Younes, Anis, & Ackerer, P. (2010). Empirical versus time stepping with embedded error
 737 control for density-driven flow in porous media. *Water Resources Research*, 46(8).
 738 <https://doi.org/10.1029/2009WR008229>
- 739 61. Younes, Anis, & Fahs, M. (2014). A semi-analytical solution for saltwater intrusion with a
 740 very narrow transition zone. *Hydrogeology Journal*, 22(2), 501–506.
 741 <https://doi.org/10.1007/s10040-014-1102-8>
- 742 62. Younes, Anis, Ackerer, P., & Delay, F. (2010). Mixed finite elements for solving 2-D
 743 diffusion-type equations. *Reviews of Geophysics*, 48(1), RG1004.
 744 <https://doi.org/10.1029/2008RG000277>
- 745 63. Zhang, D., 2002. Stochastic methods for flow in porous media: coping with uncertainties.
 746 Academic, San Diego, Calif. : London.
- 747 64. Zidane, A., Younes, A., Huggenberger, P., & Zechner, E. (2012). The Henry semianalytical
 748 solution for saltwater intrusion with reduced dispersion. *Water Resources Research*, 48(6).
 749 <https://doi.org/10.1029/2011WR011157>

750
 751
 752

